Polycomb misregulation in enterocytes drives tissue decline in the aging *Drosophila* intestine

Sarah M. Leichter[1], Kami Ahmad[1], Steven Henikoff[1,2]*

Affiliations:

[1]Basic Sciences Division, Fred Hutchinson Cancer Center, Seattle, WA, USA

[2]Howard Hughes Medical Institute, Chevy Chase, MD, USA

*Corresponding author: Email: steveh@fredhutch.org

Running title: Single-cell H3K27me3 of the aging *Drosophila* gut

Abstract

Aging compromises intestinal integrity, yet the chromatin changes driving this decline remain unclear. Polycomb-mediated repression is essential for silencing developmental genes, but this regulatory mechanism becomes dysregulated with age. Although shifts in Polycomb regulation within intestinal stem cells have been linked to gut aging, the Polycomb landscape of differentiated cell types remains unexplored. Differentiated cells comprise the majority of the gut epithelium and directly impact both tissue and whole organismal aging. Using single-cell chromatin profiling of the *Drosophila* intestine, we identify cell-type-specific chromatin landscape changes during aging. We find that old enterocytes aberrantly repress genes essential for transmembrane transport and chitin metabolism, contributing to intestinal barrier decline – an example of antagonistic pleiotropy in a regenerative tissue. Barrier decline leads to derepression of JAK/STAT ligands in all cell types and increased proliferation of aging stem cells, with elevated RNA Polymerase II (RNAPII) at S-phase-dependent histone genes. Specific upregulation of histone genes during aging stem cell proliferation resembles RNAPII hypertranscription of histone genes in aggressive human cancers. Our work reveals that misregulation of the Polycomb-mediated H3K27me3 histone modification in differentiated cells during aging not only underlies tissue decline but also mirrors transcriptional changes in cancer, suggesting a common mechanism linking aging and cancer progression.

Key words: intestinal stem cells; Polycomb domains; sciCUT&Tag; chitin synthase; chitinase; Metchnikoff

Introduction

Aging is associated with the decline of tissue function and is the leading risk factor in a multitude of diseases (Niccoli and Partridge 2012). The chromatin landscape of cells undergoes profound changes during aging, including redistribution of Polycomb-mediated repressive marks such as tri-methylation of histone H3 at lysine 27 (H3K27me3) (Emerson and Lee 2023). For example, global gains in H3K27me3 and widespread heterochromatinization have been observed in the livers of aged mice (Yang et al. 2023) and in the muscles of aging *Drosophila* (Ma et al. 2018) leading to transcriptional silencing. Forcing aged mouse liver cells to re-enter the cell cycle partially restores a youthful H3K27me3 landscape, suggesting that DNA replication may rejuvenate chromatin structure (Yang et al. 2023). However, even mitotically active somatic stem cells display age-related increases in Polycomb repression: aged *Drosophila* intestinal stem cells and mouse hematopoietic stem cells exhibit elevated dimethylation of the H3-K27 residue (H3K27me2) and H3K27me3 levels, respectively, and partial differentiation linked to these changes (Sun et al. 2014; Tauc et al. 2021).

These observations suggest that changes in Polycomb-mediated repression contribute to age-associated functional decline. Supporting this, heterozygous loss-of-function mutations in Polycomb group proteins such as the histone methyltransferase *Enhancer of zeste* (*E(z)*) lead to lifespan extension (Siebold et al. 2010), implying that Polycomb repression is detrimental in older animals. Yet, Polycomb group proteins are essential for development (Boyer et al. 2006; Blackledge and Klose 2021) and homozygous mutants are lethal (Denell and Frederick 1983) suggesting that while Polycomb activity is beneficial during development, it may become detrimental with age.

Whereas Polycomb-mediated repression appears to underlie age-associated tissue dysfunction, investigations have so far been limited to post-mitotic or stem cell systems, overlooking regenerative tissues made up of both stem and differentiated cells. The adult *Drosophila* intestine offers a model for regenerative tissues because the epithelium undergoes continuous cell turnover, with a median cellular lifespan for differentiated cells of four days (Liang et al. 2017). This rapid turnover ensures that both young and aged intestines maintain similar cellular age distributions. Despite this, the *Drosophila* intestine displays a distinctive age-related decline. Key features include barrier dysfunction, which promotes microbial dysbiosis and systemic inflammation (Rera et al. 2011; Rera et al. 2012; Martins et al. 2018; Salazar et al. 2023), as well as an increase in stem cells (Biteau et al. 2008; Rodriguez-Fernandez et al. 2020; Tauc et al. 2021). Tauc et al. demonstrated that aged intestinal stem cells mis-express lineage-specific markers via altered accessibility at Polycomb-regulated loci. However, differentiated cells comprise a majority of the epithelium (Micchelli and Perrimon 2006; Ohlstein and Spradling 2006) and defects in these cells alone have been shown to cause systemic aging (El Mai et al. 2023). Given the rapid turnover of differentiated cells, age-dependent changes in Polycomb-mediated silencing in differentiated cells could be a major driver of tissue dysfunction.

In this study we aim to test this hypothesis through single-cell profiling of the H3K27me3 mark in the *Drosophila* intestine to distinguish cell types and capture cell-type-specific dynamics of Polycomb-associated modifications during aging.

Results

Single-cell chromatin profiling of the fly gut

The epithelium of the *Drosophila* adult gut is composed of four cell types: intestinal stem cells, enteroblasts, enterocytes, and enteroendocrine cells (Micchelli and Perrimon 2006; Ohlstein and Spradling 2006). Intestinal stem cells divide symmetrically to populate the niche or asymmetrically to birth an enteroblast, an undifferentiated progenitor cell that differentiates into an enterocyte or enteroendocrine cell (Micchelli and Perrimon 2006; Ohlstein and Spradling 2006). Enterocytes are the most abundant cell type in the *Drosophila* gut and primarily function in absorption and transportation of nutrients and secretion of digestive enzymes, while enteroendocrine cells secrete gut hormones (Hung et al. 2020). Immunostaining of guts from 1-day-old *esg-GAL4, UAS-GFP* female flies, which marks intestinal stem cells/enteroblasts (ISC/EBs) with high level of GFP expression, displays distinct cell sizes and levels of GFP expression (Fig. 1A). ISC/EB cell nuclei are small with strong GFP expression, while enteroendocrine nuclei are also small with low level of GFP expression. Finally, enterocytes have large polyploid nuclei with no GFP expression. Additionally, each cell type displays distinct patterns of H3K27me3 staining, implying that gut cell types may be distinguished by chromatin landscapes of this histone modification. We used single-cell combinatorial indexing CUT&Tag (sciCUT&Tag) to barcode cells in a profiling experiment (Janssens et al. 2024). Anticipating that we would compare single cells from different ages, we dissociated guts from female flies of different ages in replicate in one experiment. We chose three ages to span adulthood in *Drosophila*: 1 day after eclosion (young), 15 days after eclosion (middle-aged), and 40 days after eclosion (old aged). Forty guts from virgin females of each age were barcoded by tagmentation, and then cells were arrayed on two ICELL8 chips for barcoded PCR (Supplemental Table S1). Peaks were called on the aggregate

data for each age using SEACR (Meers et al. 2019), then merged for dimensionality reduction and uniform manifold approximation and projection (UMAP) embedding in ArchR (Granja et al. 2021) (Supplemental Table S2). We applied multiple filtering steps to retain cells that had fragment counts of at least 100 (Supplemental Table S3), a high fraction of reads in peaks (FRiP, Supplemental Table S4) and a low fraction of blacklisted reads (Amemiya et al. 2019) (Supplemental Table S5), which after removing doublets yielded 40,982 cells for analysis.

To assign cell types using a repressive modification, we calculated chromatin silencing scores (CSS) (Wu et al. 2021), where low CSS indicates that a gene is not repressed and could be expressed, and high scores indicate a gene is repressed. Chromatin silencing scores anti-correlate with cell-type-specific gene expression profiles (Wu et al. 2021). Using ArchR for clustering and then scoring known marker genes for each cell type (Hung et al. 2020), we identified individual cells as ISC/EBs with low CSS at the escargot (*esg*) gene, enteroendocrine cells at the Piezo gene, and enterocytes at the nubbin (*nub*) gene (Supplemental Fig. S1A). We were unable to separate intestinal stem cell from enteroblasts so we group them together as an ISC/EB cluster for subsequent analyses. These three cell types form five distinct clusters on the gut UMAP; one of ISC/EBs, one of enteroendocrine cells, and three clusters of enterocytes (Fig. 1B).

First focusing on young guts, our analysis includes 11,586 young cells with 68% (7,913) of the cells called as enterocytes (Supplemental Table S6). Enterocytes have the highest fragments per cell (Fig. 1C), which might be due to more widespread repression in this cell type, and/or to polyploidy of these cells. To identify the genes repressed between cell types, we performed differential analysis for genes that fall within H3K27me3-marked

125 domains as determined using our SEACR peaks (Supplemental Tables S7-S10).
126 H3K27me3-marked domains stretch multiple kilobases in length such as the canonical
127 Antennapedia-Complex (*ANTP-C*), bithorax-complex (*BX-C*), and the Posterior sex
128 combs-Suppressor of zeste 2 (*Psc-Su(z)2*) domains (Schwartz et al. 2006), which are
129 shared across the three cell types (Fig. 1E and Supplemental Fig. S1B, C). There are
130 regions that fall outside of the canonical domains, such as at the rotund (*rn*) gene, that
131 appear to be H3K27me3-marked in enteroendocrine and ISC/EBs, but not enterocytes
132 (Fig. 1E), indicating differences in the H3K27me3 landscape between the cell types. Of
133 the 8,697 genes in domains, 10.7% (933) show differential signal between the young cell
134 types from differential analysis (Fig. 1D and Supplemental Table S11). Genes in cell-type
135 specific domains include the *42AB* piRNA cluster (Fig. 1F), which is positively regulated
136 by the H3K27me3 modification in *Drosophila* ovarian stem cells (Akkouche et al. 2025),
137 but is expressed at low levels in the gut (Siudeja et al. 2021). In differentiated cells, the
138 non-coding RNA lncRNA:CR32773 forms an H3K27me3 domain in enteroendocrine cells
139 (Fig. 1G) and held out wings (*how*) is H3K27me3-marked in enterocytes (Fig. 1H). Some
140 genes are marked with the H3K27me3 modification in two cell types but not the third:
141 enterocytes and enteroendocrine cells share a greater number of common H3K27me3-
142 marked genes with ISC/EBs (122 genes, cluster 6 and 191 genes, cluster 5, respectively)
143 than they do with each other (51 genes, cluster 1) (Fig. 1D). We interpret this pattern as
144 evidence of lineage-specification, where differentiated cells retain H3K27me3 marks from
145 their cell of origin (ISC/EBs) and therefore resemble progenitors more closely than they
146 resemble each other. We conclude that sciCUT&Tag effectively separates the cell types
147 of the gut and identifies repressed domains characteristic of each cell type.

Gains and losses of repression in aging cells

Next, coloring the gut H3K27me3 single-cell UMAP (Fig. 1B) based on the three ages of each cell type reveals that ISC/EBs of different ages are intermixed, as are enteroendocrine cells (Fig. 2A, B). This indicates relatively small changes to the chromatin landscapes of these two cell types as animals age. Enterocytes from each age form distinct clusters (Fig. 2C), implying that the chromatin landscape of this cell type changes drastically with age. We also compared fragment counts per cell across ages and lineages, which showed a modest but significant increase with age (Supplemental Fig. S2).

To map age-dependent changes in H3K27me3 landscapes for each cell type, we performed differential analysis between young and old clusters (Supplemental Table S12-S14). We identified 75 genes where H3K27me3 changes in ISC/EBs (Fig. 2D), 277 genes in enteroendocrine cells (Fig. 2E), and 1588 genes in enterocytes (Fig. 2F). Among the genes that lose H3K27me3 signal in both ISC/EBs and enteroendocrine cells, GO analysis revealed enrichment for transcriptional regulators and RNA Polymerase II (RNAPII) associated functions (Supplemental Fig. S3A ,B, Supplemental Tables S15, S16). This included derepression of multiple transcription factor genes such as worniu (*wor*) in ISC/EBs and Ets at 21C (*Ets21C*) in enteroendocrine cells, which are involved in stem cell proliferation and fate decisions (Supplemental Fig. S3C, D).

In enterocytes, we observed both gains and losses of H3K27me3 with age, where 710 genes decreased in H3K27me3 signal while 878 increased in H3K27me3 signal. The genes that decreased in H3K27me3 signal with age are strong domains in young cells. For example, a domain encompassing the pointed (*pnt*) and oo18 RNA-binding protein

(*orb*) genes loses the H3K27me3 mark (Fig. 2G). By contrast, genes that gained H3K27me3 signal with age are weak domains in young cells. An example of this is the Multi drug resistance 50 (*Mdr50*) gene (Fig. 2H), which encodes an efflux transmembrane transporter expressed in the midgut involved with xenobiotic transport activity and response to insecticide (Denecke et al. 2017). These findings suggest that aging not only weakens pre-existing Polycomb domains but also establishes new repressive marks in differentiated intestinal cells, reshaping the chromatin landscape in a cell-type-specific manner.

Changes in repression at regulatory elements with age

A major advantage of sciCUT&Tag is the ability to directly profile changes at regulatory elements, which single-cell RNA sequencing (scRNA-seq) does not capture. To identify regulatory elements that exhibit changes in H3K27me3 level with age within each cell type, we identified self-transcribing active regulatory region sequencing (STARR-seq) enhancers (Zabidi et al. 2015) that fell within our list of H3K27me3 peaks, acknowledging that this list may miss gut-specific sites. From differential analysis, we identified 18 enhancers that changed with age in ISC/EBs and 406 in enterocytes, but none in enteroendocrine cells (Supplemental Fig. S4A, B; Supplemental Tables S17, S18).

Next, we searched for transcription factor motifs within enhancers that significantly change within each cell type using FIMO (Grant et al. 2011) against the JASPAR insect transcription factor database (Rauluseviciute et al. 2024). We find in aged ISC/EBs, enhancers that lose H3K27me3 are enriched for motifs linked to chromatin organization and developmental regulation (e.g., Chromatin-linked adaptor for MSL proteins (CLAMP), snail (sna), buttonhead (btd), and Kr transcription factor (Kr)) (Supplemental Fig. S4C).

In contrast, those that gain H3K27me3 signal show motifs for developmental regulators such as twist (twi), hb transcription factor (hb), and tinman (tin) (Supplemental Fig. S4D). In enterocytes, motifs for stress-responsive TFs and motifs for Trithorax-like (Trl) and grainy head (grh), which are known to influence enhancer accessibility, dominate in enhancers losing H3K27me3 signal (Supplemental Fig. S4E). At the same time, architectural proteins such as CTCF and Motif 1 Binding Protein (M1BP) are enriched in enhancers that gain H3K27me3 signal with age (Supplemental Fig. S4F). Notably, CLAMP motifs appear consistently across cell types, enriched in enhancers that both lose and gain H3K27me3 signal with age. CLAMP has been shown to displace Trl/GAF during stress and act as a transcriptional repressor (Aguilera et al. 2025). Together, these findings suggest that CLAMP functions in a context-dependent manner during aging, contributing to both repression and derepression of enhancer activity under stress-associated conditions. These results point to chromatin-level changes that may prime these cells for altered transcriptional programs with age.

Polycomb repression of barrier membrane genes in aging enterocytes

A major defect of the aging *Drosophila* gut is breakdown of the protective barrier membrane (Salazar et al. 2023). This is observed through the ‘Smurf Assay’ in which flies are fed food containing a non-absorbable blue dye that stains only the digestive tract of young flies where the intestinal barrier is intact, but in old flies the blue dye spreads through the whole body due to increased permeability of the gut (Rera et al. 2011; Rera et al. 2012; Martins et al. 2018) (Fig. 3A). Given that elevated H3K27me3 levels have been associated with reduced lifespan (Siebold et al. 2010; Ma et al. 2018), we

hypothesized that age-related changes in the H3K27me3 landscape of enterocytes may contribute to barrier dysfunction.

To investigate this, we performed GO analysis of genes that gain or lose H3K27me3 signal in aged enterocytes (Supplemental Tables S19, S20). Among the genes that lose H3K27me3 signal with age, top GO terms include “neurogenesis”, “regulation of transcription by RNA Polymerase II”, “generation of neurons”, and “transcription by RNA Polymerase II” (Supplemental Fig. S5A), which resulted in a list of transcription factor genes involved in development and differentiation that become derepressed with age (Supplemental Fig. S5B). Notably, this group includes the Enhancer of Split (*E(spl)*) complex genes, located on Chromosome *3R*, which are normally Polycomb-repressed in young enterocytes (Josserand et al. 2023) (Supplemental Fig. S5C) as well as the HOX transcription factor paired (*prd*) (Supplemental Fig. S5D). These findings mirror the chromatin derepression of transcription factor genes in aged ISC/EBs and enteroendocrine cells, consistent with a widespread relaxation of lineage-specific repression programs during aging.

In contrast, GO analysis of genes that gain H3K27me3 signal in aged enterocytes reveal enrichment for the terms “transmembrane transport”, “tissue morphogenesis”, “morphogenesis of an epithelium”, and “aminoglycan metabolic process” (Fig. 3B). Of particular interest is this last term, as the barrier that forms over the intestinal epithelium protecting it from contents from the lumen, the peritrophic matrix, is composed of the aminoglycan chitin (Lehane 1997). The peritrophic matrix of insects is analogous to the mammalian mucus-based membrane of the digestive track (Konno and Mitsuhashi 2019), is produced in the foregut, and midgut enterocytes produce chitin to maintain the

peritrophic matrix (Dutta et al. 2015; Zhu et al. 2024). Disruption of chitin secretion from enterocytes to the peritrophic matrix leads to barrier dysfunction and susceptibility to stress (Katheder et al. 2023). Two gut-specific genes that acquire strong H3K27me3-marked domains in aged enterocytes are Chitin synthase 2 (*Chs2*) and Chitinase 9 (*Cht9*) (Fig. 3C, D). Both of these genes are involved in maintenance of the peritrophic matrix and in the midgut are expressed in enterocytes (Supplemental Table S21) (Buchon et al. 2013; Hung et al. 2020). Degradation of chitin and silencing of *Chs2* are key targets for the development of insecticides against pests such as mosquitos (Zhang et al. 2023). *Cht9* is specifically expressed in the gut (Leader et al. 2018; Krause et al. 2022) but is clustered together with three other chitinases (Chitanse *8* (*Cht8*), Chitinase 12 (*Cht12*), and Chitinase 4 (*Cht4*)) that all become marked with H3K27me3 with age (Fig. 3D). The H3K27me3 domains only form over *Chs2* and the *Cht4-8-9-12* chitinase gene clusters in aged enterocytes, implying that they become repressed in older animals (Supplemental Fig. S6A, B).

To determine if the increase in H3K27me3 signal across the domain leads to transcriptional silencing of *Chs2* and *Cht9*, we profiled the initiating serine-5 phosphorylated isoform of RNA Polymerase II (RNAPIIS5P) in whole guts using CUT&Tag under CUTAC low-salt tagmentation conditions (Henikoff et al. 2020; Janssens et al. 2022) (Supplemental Tables S1, S22). RNAPIIS5P provides a direct view of ongoing transcriptional engagement and promoter-proximal regulation that RNA-seq does not capture.

Previously published single-cell RNA-seq data from the aging Drosophila intestine (Tauc et al. 2021) were generated from FACS-isolated cells, resulting in datasets heavily

enriched for ISCs and EBs, with few differentiated cells represented (Supplemental Table S23). In contrast, our single-cell H3K27me3 and bulk RNAPII-S5P datasets were generated from whole guts without cell sorting. Because of these fundamental differences in sample composition and experimental design, the published single-cell RNA-seq data are not directly compatible for integration with our H3K27me3 sciCUT&Tag dataset.

We performed four replicates of RNAPIIS5P CUTAC per age and identified a high Pearson's correlation between replicates within an age group, allowing us to merge the four replicates for analysis (Supplemental Fig. S7). We found that RNAPIIS5P is present at the promoters of the *Chs2, Cht4 and Cht9* genes in young tissues and lacking at *Cht12*, which is not expressed in this tissue (Leader et al. 2018; Krause et al. 2022). For the three genes that are expressed, signal decreases with age (Fig. 3E, Supplemental Fig. S8A, B, confirming that these genes become repressed. From differential analysis between young and old guts, *Chs2* and *Cht9* are significantly repressed with age (Supplemental Table S24).

We next asked why H3K27me3 would accumulate over chitin genes with age. The H3K27me3 mark is bound by the Polycomb chromodomain protein (Pc) (Cao et al. 2002), but Pc is also localized at the promoters of many active genes (Orsi et al. 2014). Given the duality of Pc binding, we profiled the Pc protein in all three ages of whole guts by CUT&Tag (Supplemental Tables S1, S25). We found that Pc binds promoters both within and outside of H3K27me3-marked domains identified across all three cell types and ages. In the intestine, a larger fraction of promoters fall within H3K27me3-marked domains because cells of this tissue exhibit more broadly repressed chromatin than previously profiled Drosophila tissues (Supplemental Fig. S9A, B). Genome-wide analyses have

shown that the majority of Pc binding sites in other Drosophila tissues are located outside of H3K27me3-marked domains (Orsi et al. 2014; Loubiere et al. 2016; Brown et al. 2018). Promoter-proximal Pc sites outside of H3K27me3 domains differ from Pc occupancy within domains, where Pc is predominantly anchored at Polycomb Response Elements (PREs).

We observe minimal changes in Pc signal across ages (Supplemental Fig. S9A, B). For example, the H3K27me3 domain around the gene senseless-2 (*sens-2*) is present in all three cell types and contains multiple Pc binding sites that are stable with age (Supplemental Fig. S9C). In contrast, Sphingosine-1-phosphate lyase (*Sply*) lacks the H3K27me3 mark and is therefore not located within a domain but is bound by Pc (Supplemental Fig. S9D), consistent with prior reports that Pc can localize independently of H3K27me3 (Schaaf et al. 2013; Orsi et al. 2014; Loubiere et al. 2016).

When we examined Pc level at the promoters of chitin genes we found that it is present around the active promoters of the *Chs2* and *Cht9* genes in young guts (Fig. 3F, G) and in older tissues (Fig. 3H, Supplemental Fig. S7C, D), with high specificity compared to the promoters of genes lacking Pc signal, such as the promoters of the genes radish (*rad*) and dusky (*dy*) (Supplmental Fig. S8E, F). Although the signal at *Cht9* appears low, it is exhibits a level of signal greater than IgG, which is a non-specific antibody that serves as a control for CUT&Tag (Kaya-Okur et al. 2019; Kaya-Okur et al. 2020) (Supplemental Table S26). In a coverage heatmap ordered by Pc descending signal, we find *Chs2* and *Cht9* to be present in the top 25% of promoters within H3K27me3 domains (Supplemental Figure S8A). Thus, while the presence of Pc at these promoters is compatible with gene expression in young tissues, in aged guts binding of the Pc chromodomain to H3K27me3

leads to chromatin compaction and gene repression (Kassis et al. 2017). Note, we find that many Pc binding sites do not trigger the formation of a H3K27me3 domain with age (Supplemental Figure S9B, D). Therefore, we hypothesize that using Pc for gene regulation early in life comes with the risk of nucleating repression later in life.

Derepression of enteroendocrine genes in aged guts

Having established that age-dependent H3K27me3 gain in enterocytes drives barrier failure, we next asked how Polycomb changes in the aged ISC/EB lineage. Previous studies have reported an age-related increase in enteroendocrine precursor cells, identified by co-expression of intestinal stem cell and enteroendocrine markers, which is linked to changes in chromatin accessibility of Polycomb-regulated loci (Tauc et al. 2021). Using the set of genes marked by H3K27me3 in young enteroendocrine cells from differential analysis (Fig. 1D), we find that aged ISC/EBs gain H3K27me3 signal over many enteroendocrine-marked genes (124 of 205) including Nopp140*,* warts (*wrts*)*,* and Drip (Fig. 4A), indicating that aged ISC/EBs begin to acquire an H3K27me3 landscape that partially resembles that of enteroendocrine cells, although these cells still cluster with ISC/EBs in our UMAP (Figure 2A). We also observed the loss of signal at a subset of H3K27me3-marked enteroendocrine genes in aged ISC/EBs, including transcription factors such as *Ets21C* and invected *(inv*), and the slit receptor roundabout2 (*robo2*) (Fig. 4A). *Robo2* restricts ISC commitment to the enteroendocrine lineage through repression of prospero (Biteau and Jasper 2014). The loss of H3K27me3 at *robo2* in aged progenitor cells may reflect a compensatory mechanism that preserves some stem cell identity by restricting full differentiation into the enteroendocrine lineage. This suggests that aged ISC/EBs adopt a chromatin landscape partially resembling that of enteroendocrine cells,

consistent with the model in which aged stem cells exhibit partial differentiation toward the enteroendocrine fate (Tauc et al. 2021). To further support this conclusion, we examined additional genes in aged ISC/EBs that have been identified as markers of enteroendocrine precursors and neural stem cell potential, including *sna*, *wor*, and *deadpan* (*dpn*) (Tauc et al. 2021). These genes lose H3K27me3 signal in aged ISC/EBs (Supplemental Fig. S10), reinforcing the model that aging pushes progenitor cells toward partial differentiation into the enteroendocrine lineage.

JAK/STAT ligands become derepressed in aged gut

Over-proliferation of stem cells (Biteau et al. 2008) is reflected in the higher abundance of ISC/EBs in older guts (Fig. 4B). Indeed, the proportion of stem cells based on single-cell profiling increases from 22.4% in young tissues to 52.5% in aged tissues (Fig. 4C). Stem cell over-proliferation is stimulated by production of Unpaired ligands which activate the JAK/STAT pathway (Jiang et al. 2009). We observe that this domain loses the H3K27me3 mark in all three cell types (Fig. 4D, Supplemental Fig. S11A). This loss is accompanied by an increase in RNAPIIS5P signal at the unpaired 3 (*upd3*) promoter, which is statistically significant by differential analysis (Fig. 4E, Supplemental Fig. S11B, Supplemental Table S24), the unpaired gene specifically expressed in the gut (Jiang et al. 2009). The unpaired 2 (*upd2*) promoter also shows increased RNAPII-S5P with age (Fig. 4E, Supplemental Fig. S11C). By contrast, the unpaired 1 (*upd1*) promoter maintains very low RNAPII-S5P at all ages, consistent with persistent H3K27me3 signal over the *upd1* gene in all ages and cell types (Supplemental Fig. S11A, D). Expression of these ligands is known to be regulated by Polycomb silencing, as knockdown of Polycomb silencing components leads to loss of the H3K27me3 mark over a domain encompassing

the three unpaired genes, resulting in increased expression and to tumor formation (Parreno et al. 2024). Additionally, we observe increased RNAPIIS5P at the promoters of the JAK/STAT target genes Zinc finger homeodomain 1 (*zfh1*) and 2 (*zfh2*) (Supplemental Fig. S11E, F). These results support the idea that as the gut ages, damaged enterocytes induce derepression of JAK/STAT ligands, leading to over-proliferation of stem cells and hyperplasia of the tissue.

S-phase-dependent histone gene upregulation with cell proliferation

The increase in ISC/EB cell number prompted us to test for global gene upregulation, or hypertranscription, a general feature of mammalian stem cell proliferation (Kim et al. 2023; Kim et al. 2024). We previously showed that hypertranscription can be detected in cancer by plotting the difference in RNAPIIS5P signal between tumor and normal cells as a function of the average RNAPIIS5P signal (Henikoff et al. 2025). We applied the same analytical approach to *Drosophila* gut samples, for each promoter plotting the RNAPIIS5P difference between each age as a function of the average signal (Altman and Bland 1983) displayed on a $\log_{10}$ scale for clarity. Excluding histone genes, neither hyper- nor hypotranscription was observed for the 15- to 1-day comparison (Supplemental Fig. S12A), although hypotranscription was detected between 40- and 15-day-old and 40- and 1-day-old guts (Figure 5A, Supplemental Fig. S12B). The multiple-copy histone genes were exceptional, displaying enormous enrichment of RNAPIIS5P at the multiple-copy S-phase-dependent core histone genes, greater enrichment for His2A, His2B, His3 and His4 than for all 21,876 other annotated promoters (Fig. 5A, Supplemental Fig. S12A, B). By contrast, histone H1, the linker histone responsible for primary chromatin compaction, showed lower level of enrichment with age (Figure 5B, Supplemental Fig. S12B).

Importantly, S-phase-dependent histone transcripts lack polyadenylation (Marzluff and Koreski 2017) and are poorly captured by standard RNA-seq, making RNAPIIS5P profiling especially suitable for assessing their transcriptional regulation. Direct comparison of 40 days old versus 15 days old tissues show widespread loss of RNAPIIS5P at most genes, accompanied by orders-of-magnitude higher levels at histone loci (Figure 5B, C). Notably, 15 days old corresponds to the peak of gut maturation, after which age-related decline begins (Capo et al. 2019). This establishes S-phase-dependent histone gene upregulation as a transcriptional signature of advanced aging in this tissue.

RNAPII accumulates at histone genes during times of rapid cell proliferation such as in early *Drosophila* embryos (Huang et al. 2021) and in mouse embryonic stem cells at S-phase (Mahat et al. 2024) with corresponding reductions genome-wide. As S-phase-dependent histones are rate-limiting for proliferation, their specific accumulation of RNAPIIS5P is consistent with histone gene transcription driving stem cell over-proliferation in the gut. Whereas RNAPIIS5P increases at all four core histone genes in old tissue, the genes for histone His2B and for histone His2A increase the most (Fig. 5C, D), suggesting a higher demand for these histones in the aging gut. In yeast, overexpression of core histone genes extends replicative lifespan, highlighting their potential role in promoting cellular longevity (Feser et al. 2010). Increased RNAPIIS5P at S-phase-dependent histone genes during aging-associated stem cell proliferation resembles similar upregulation at orthologous histone genes in other rapidly dividing cell types.

Discussion

Over a century ago Elie Metchnikoff hypothesized that systemic aging results from the breakdown of the intestinal barrier (Metchnikoff and Mitchell 1907; Salazar et al. 2023), with toxic effects inducing aging of other tissues (Rera et al. 2012). Our study provides a chromatin-level mechanism for this hypothesis by showing that age-dependent gains of the repressive H3K27me3 mark in enterocytes—and corresponding losses at other loci—alter gene expression programs that underlie gut aging. Enterocytes accrue ectopic H3K27me3 signal over multiple chitin-synthesis genes, compromising the peritrophic matrix that normally shields the epithelium from luminal toxins (Zhang et al. 2023). Consistent with analogous zebrafish studies showing that enterocyte-specific telomerase loss drives systemic aging and that its restoration slows organismal decline (El Mai et al. 2023), our results underscore enterocytes as critical drivers of aging. Although previous *Drosophila* studies attributed gut aging to chromatin changes in intestinal stem cells (Tauc et al. 2021), our results position enterocytes as the initiating cell type: by repressing chitin-related genes, aged enterocytes drive barrier failure, stem-cell hyperproliferation, and likely systemic aging effects (Fig. 6). Loss of barrier integrity is not only a hallmark of gut aging but also a strong predictor of imminent death (Rera et al. 2012) as toxins leaking into circulation promote microbial dysbiosis, systemic inflammation, and lifespan limitation (Clark et al. 2015; Li et al. 2016; Salazar et al. 2023).

Why would chitin synthesis genes acquire Polycomb repression in aged animals? Polycomb repression is mediated by the PRC2 complex, which methylates H3K27 on nucleosomes. The chromodomain of Polycomb (Pc) protein component of PRC1 specifically binds H3K27me3, but Pc also binds at active promoters (Schaaf et al. 2013; Orsi et al. 2014). We propose that the binding of Polycomb at active promoters carries a

risk, at some low frequency, of nucleating repression. Polycomb protein occupies the promoters of both the *Chs2* and *Cht9* genes in guts, and so as animals age stochastic nucleation of repression would silence these critical genes, resulting in peritrophic membrane breakdown and leaky guts.

Normal Polycomb regulation in young adult *Drosophila* but aberrant mis-regulation in aged flies may be a molecular example of antagonistic pleiotropy. In this evolutionary framework, genes beneficial to the organism early in life are selected for, regardless of any deleterious consequences they may have later in life (Williams 1957). This framework explains aging not as the inevitable breakdown of living machinery, or as a necessary programmed stage of life history, but as the unselected side-effect of pleiotropic genes selected for their early benefits. One such example of antagonistic pleiotropy has been documented in the nematode *Caenorhabditis elegans*, where insulin signaling stimulates reproduction early in life but also shortens lifespan (Jenkins et al. 2004). In this case early reproduction is selected for; side-effects on lifespan are irrelevant. Antagonistic pleiotropy of Polycomb regulation may also explain why genetic reduction of Polycomb components extend lifespan in *Drosophila* (Siebold et al. 2010), perhaps simply by reducing silencing of chitin synthesis genes in old enterocytes.

We also identified a small number of significant changes to the H3K27me3 landscape in aged ISC/EBs, including derepression of enteroendocrine marker genes, consistent with a prior report of partial differentiation of this cell type with age through Polycomb silencing (Tauc et al. 2021). It is unclear if skewed lineage commitment is a cause or consequence of the accumulation of defective enterocytes in aged tissues. Thus, we attribute aging in the gut to the aberrant Polycomb silencing in enterocytes, which results in stimulation of

stem cells to divide, leading to increased RNAPIIS5P occupancy at the histone genes (Fig. 6). While defective enterocytes may be the proximal cause of gut permeability, the induction of compensatory stem cell proliferation may be responsible for other age-related syndromes.

Notably, cancer risk is strongly associated with age (Havas et al. 2022), and reduced stem cell proliferation reduces this risk (Zhuang et al. 2025). In contrast to cancer, aged guts do not show hypertranscription but rather exhibit a selective increase in RNA Polymerase II occupancy at histone genes, likely driven by stem cell hyper-proliferation. Other genes appear to lose RNA Polymerase II occupancy. The loss at other genes may be due to changes in cell type proportions with age; however, we cannot confirm this without cell-type-specific RNAPIIS5P profiles. Regardless, we observe high levels of RNAPIIS5P at the histone genes in old tissues, suggesting old ISC/EBs overexpress these genes. We previously demonstrated that increased levels of RNA Polymerase II at histone genes predicts outcome and correlates with whole-arm chromosomal losses in human cancer (Henikoff et al. 2025; Zheng et al. 2025), suggesting a causal role of increased RNAPIIS5P occupancy at the histone genes cancer development and aging tissues that exhibit stem cell over-proliferation.

Materials and Methods

Fly Husbandry

The *esgGal4/CyO; UAS-GFP/TM6B* strain was a gift from Bruce Edgar. All flies used for chromatin profiling in this study were of the w^{1118} genotype and were maintained at 25˚C.

Virgin females were collected and were kept in uncrowded conditions of 15 or less flies per vial, being flipped every other day to maintain adequate food supply.

Antibodies

Primary antibodies: Anti-H3K27me3: Cell Signaling Technologies cat. no. 9733, lot 19; Anti-RNAPIIS5P: Cell Signaling Technologies cat. no. 13523, lot 3; Anti-Pc: a gift from Judith Kassis; Anti-IgG: Abcam cat. no. ab46540; Anti-GFP: Thermo Fisher Scientific cat. no. 3E6. Secondary antibodies: Guinea pig α-rabbit antibody Antibodies online cat. no. ABIN101961, lot 46671; Anti-mouse-FITC: Jackson Immuno Research cat. no. 115-095-166; Anti-rabbit-Texas Red: Jackson Immuno Research cat. 111-585-144.

Imaging Immunostained guts

Guts from one-day old or forty days old adult females of genotype *esgGal4/CyO; UAS-GFP/TM6B* were dissected, incubated in Accutase (Stem Cell Technologies cat. 07922) for 10mins, and fixed in 4% formaldehyde/PBS with 0.1% Triton X-100 (PBST) for 10 minutes, incubated in 0.3% sodium deoxycholate/PBST 2× for 10 minutes twice (Lim and Fuller 2012), and then incubated with primary antibodies (1:100 dilution) in Goat Serum (Fisher Scientific cat. 16-210-072) in PBS buffer at 4°C overnight and then with fluorescently-labeled secondary antibodies (1:200 dilution, Jackson ImmunoResearch) for two hours at room temperature. Guts were stained with 0.5 µg/mL DAPI/PBS and mounted in 80% glycerol on slides and imaged by epifluorescence on Leica Stellaris8 Confocal at the Fred Hutch Cellular Imaging Shared Resource and processed using Fiji software (Schindelin et al. 2012).

Smurf Assay

The Smurf assay was conducted as previously described in (Martins et al. 2018). Smurf food was prepared by adding non-absorbable blue dye (FD&C Blue No. 1, Sigma-Aldrich, catalog number: 861146) to standard fly food at a final concentration of 2.5% (w/v). Virgin female flies were collected and maintained at a density of 20 flies per vial. Flies were monitored daily for signs of "Smurfness" (blue dye outside of the digestive tract indicating intestinal barrier failure) and survival. Flies were flipped daily on to fresh Smurf food.

SciCUT&Tag library preparation

40 midguts per age were dissected in 1× PBS, working 10 at a time and moving into a 1.5mL tube containing 1× PBS on ice during processing. Once 40 midguts of one age were dissected, they were moved to a petri dish in a drop of 1× PBS on ice and chopped with a razor. Chopped up tissue was moved to a tube containing 160 µL of 2mg/mL collagenase (Millipore Sigma cat # C9407) with 50 mM HEPES and 360 µM $CaCl_2$ for 1 hour at room temperature with gentle vortexing every 15 minutes. We then added 10uL of 0.5M EDTA to inhibit the collagenase and spun down the samples at 600×g for 3mins and removed the supernatant. The remainder of the procedure was performed following the sciCUT&Tag protocol described in (Janssens et al. 2024). Two iCell8 chips (TaKaRa, cat. no. 640019) were ran and sequenced on Illumina NextSeq 2000 using a the P1-100 flow cell at Fred Hutchinson Cancer Center Genomics Shared Resource.

Bulk Chromatin Profiling

We dissected guts from female flies of 1, 15, and 40 days old in 1× PBS, working 10 at a time and moving into a 1.5mL tube containing 1× PBS on ice during processing. Four replicates per age per epitope of profiling reactions were performed, with 5 guts per

reaction. Each sample was digested in 50 µL of 2mg/mL collagenase (Millipore Sigma cat # C9407) containing 50 mM HEPES and 360 µM $CaCl_2$ 1hr at room temperature with gentle vortexing every 15 minutes. After dissociation, 5uL of Concanavalin-A-conjugated magnetic beads (ConA beads, Bangs Laboratories cat #BP531) were added and allowed to bind at room temperature for 10 minutes. Buffer exchange was performed on a magnetic stand (MACSiMAG Seperator cat #130-092-168). Bead-bound cells were incubated with primary antibody in Wash buffer (20 mM HEPES pH 7.5, 150 mM NaCl, 0.5 mM spermidine, 0.05% Triton X-100 and Roche EDTA-free protease inhibitor) overnight at 4°C, incubated with secondary antibody in Wash buffer for 1 hour at room temperature, and then incubated with protein-A-Tn5 loaded with adapters (Epicypher cat #15-1117) in 300-Wash buffer (20 mM HEPES pH 7.5, 300 mM NaCl, 0.5 mM spermidine, 0.05% Triton X-100 with Roche cOmplete protease inhibitor) for 1 hour. After one wash with 300Wash+ buffer, samples were incubated in CUTAC-DMF Tagmentation buffer (10 mM TAPS, 5 mM $MgCl_2$, 20% DMF, 0.05% Triton X-100) for 30 minutes at 37 °C. After tagmentation, samples were washed with TAPS wash buffer (10 mM TAPS, 0.2 mM EDTA). Fragment release was performed in 5 µl 1% SDS supplemented with 1:10 Thermolabile Proteinase K (New England Biolabs cat. no. P8111S) at 37 °C for 1 hour followed by 58˚C for 1 hour SDS was quenched by addition of 15 µl 6% Triton X-100 and PCR was performed by addition of 2 µl each barcoded 10mM i5 and i7 primer solutions and 25 µl NEBNext 2× PCR Master mix (New England Biolabs cat. no. ME541L). Libraries were prepared as described (Kaya-Okur et al. 2019; Henikoff et al. 2020) with 14 cycles of PCR with 10 second combined annealing and extension for enrichment of short DNA fragments. Libraries were pooled by volume by epitope and were sequenced in PE50

mode on the Illumina NovaSeq X platform at the Fred Hutchinson Cancer Center Genomics Shared Resource.

Statistics and computational analyses

Single-cell sequencing analysis

Demultiplexing was performed using the sciCTextract custom software (https://github.com/mfitzgib/sciCTextract) (Janssens et al. 2024). Adapter sequences were cut using cutadapt 2.9 (Martin 2011) with parameters: -j 8 -m 20 -a CTGTCTCTTATACACATCT -A CTGTCTCTTATACACATCT -Z. Sequences were aligned using Bowtie 2 (Langmead and Salzberg 2012) version 2.4.2 to dm6 with parameters: –very-sensitive-local –soft-clipped-unmapped-tlen –no-mixed –no-discordant –dovetail –phred33 -I 10 -X 1000. SAM file created by Bowtie 2 was converted to a BAM file and run 'bedtools bamtobed -bedpe' (Quinlan 2014) on the resulting BAM file. For input into the single-cell analysis software ArchR (Granja et al. 2021), we extracted columns 1, 2, 6 and 7 of the BED files, which correspond to the chr, start, end and the rewrote the headers to include the barcode. Then the BED files were further processed by reformatting the fourth column to include just the barcode sequence and removing duplicate reads with the same Chromosome, start, stop, and barcode (Janssens et al. 2024). We chose to use the 'peakmatrix' option in ArchR to generate the LSI, so to call peaks we merged BAM files from the two iCell8 wafers for each age and used the pseudo-bulk as input into SEACR using the stringent parameter and a cutoff of FDR < 0.01 (Meers et al. 2019) (Supplemental Table S2). Peaks for each age were merged using 'bedtools merge'. We then made the following cutoffs of our data in ArchR: keeping cells with at least 100

fragments/cell, keeping cells with only a FRIP of 0.7 and greater, and removing cells with a fraction of reads that fell into the blacklist (Amemiya et al. 2019) that was greater than 0.2 (Supplemental Tables S3-S5). 100 fragments per cell represents a sequencing depth of 0.000056X coverage per cell for the Drosophila genome, which is greater than what has been reported previously for single-cell CUT&Tag (Wu et al. 2021). We then removed doublets using the ArchR addDoubletScores and filterDoublets functions (Granja et al. 2021). For graph-based clustering of sciCUT&Tag data, we used the approach implemented in Seurat (Butler et al. 2018), and then compared common metrics across clusters, including information content (reads/cell) and gene coverage. To annotate cell types using H3K27me3, we calculated chromatin silencing scores as previously reported (Wu et al. 2021). CSS are gene-level, distance-weighted aggregation of single-cell H3K27me3 signal using the ArchR gene activity/score model**,** which converts fragment counts in tiles around each gene into a depth-normalized score. For H3K27me3, high coverage indicates a 'repressed' status, whereas low coverage indicates 'unrepressed'.

Once we had annotated the three cell types (ISCs and EBs were too similar separate into distinct clusters), we exported the barcodes from ArchR and using grep commands, pulled out the fragment information for each cell of each cell type for each age. We then created count tables from the cell-type-specific fragment files using 'bedtools intersect -c' against genes within SEACR peaks (Supplemental Tables S7-S10). Count tables were uploaded to the Degust server (https://degust.erc.monash.edu/) for differential analysis (Supplemental Tables S11-S14). Normalized counts from the count tables were used to generate heatmaps using *ggplot2* (Wickham 2016) in R (R Core Team 2025) for visualization. GO analysis was performed using clusterProfiler (Yu et al. 2012) and

visualized using *ggplot2* (Wickham 2016) in R (R Core Team 2025) (Supplemental Tables S15, S16). BED files from each iCell8 chip were merged and created into normalized count bigwigs by BEDTools (v2.30) (Quinlan 2014) genomecov command with scale (size_of_reference_sequence/total_counts). Normalized count bigwigs are the fraction of counts at each base pair scaled by the size of the reference sequence so that if the counts were uniformly distributed across the genome there would be one at each position. Tracks were uploaded to UCSC Genome Browser and then downloaded as PDF files. For analysis of enhancer regions, a list of curated enhancers from *Drosophila* (Zabidi et al. 2015) was downloaded and then filtered for enhancers that fell within our list of H3K27me3 peaks using 'bedtools intersect' (Quinlan 2014). We then created count tables for enhancers within peaks from the cell-type-specific fragment files using 'bedtools intersect -c'. Count tables were uploaded to the Degust server (https://degust.erc.monash.edu/) for differential analysis (Supplemental Tables S17, S18). Differentially enriched enhancers were then used for motif searching using FIMO (Grant et al. 2011) and a list of known transcription factor motifs from JASPAR insect database (Rauluseviciute et al. 2024). Heatmaps and dot plots were generated in R (R Core Team 2025) using *ggplot2* (Wickham 2016).

Bulk sequencing analysis

Adapters were clipped using cutadapt 4.1 with the following parameters: -j 8 --nextseq-trim 20 -m 20 -a AGATCGGAAGAGCACACGTCTGAACTCCAGTCA -A AGATCGGAAGAGCGTCGTGTAGGGAAAGAGTGT -Z. Paired-end reads were mapped to a repeat masked release r6.30 of the *D. melanogaster* genome obtained from UCSC (http://hgdownload.cse.ucsc.edu/goldenPath/dm6/bigZips/dm6.fa.masked.gz) using

Bowtie 2 using the following parameters: --very-sensitive-local --soft-clipped-unmapped-tlen --dovetail --no-mixed --no-discordant -q --phred33 -I 10 -X 1000.

Properly paired reads were extracted from the alignments by SAMtools (v1.14) (Danecek et al. 2021) bamtobed command into mapped fragment BED files. Replicate BED files were merged and created into normalized count bigwigs by BEDTools (v2.30) genomecov command with scale (size_of_reference_sequence/total_counts). Normalized count bigwigs are the fraction of counts at each base pair scaled by the size of the reference sequence so that if the counts were uniformly distributed across the genome there would be one at each position. Comparisons between Pc and IgG signal for promoters in Supplmental Table S25 was performed using normalized count bigwigs using UCSC tools BigWigAverageOverBed (Kent et al. 2010).

Count tables were generated using BED files using 'bedtools intersect -c' against promoter list of the dm6 genome version 31 downloaded from FlyBase. Normalized counts from the count tables were used to generate heatmaps using *ggplot2* in R (R Core Team 2025) for visualization (Supplemental Tables S22, S23) (Wickham 2016). Aggregate plots with heatmaps were generated using deepTools2 (Ramirez et al. 2016).

Data access:

All raw and processed sequencing data generated in this study have been deposited in the NCBI Gene Expression Omnibus (GEO; https://www.ncbi.nlm.nih.gov/geo/) database undeaccession code GSE291173. sciCTextract custom software for demultiplexing sciCUT&Tag can be found on GitHub (https://github.com/mfitzgib/sciCTextract).

Competing interest statement:

K.A. and S.H. have filed patent applications on related work. The other authors declare no competing interests.

Acknowledgements

We thank C. Codomo, J. Henikoff, and M. Fitzgibbons for technical assistance, the Fred Hutchinson Cancer Center Genomics Shared Resource for sequencing and data processing, and at Fred Hutchinson Cancer Center Cellular Imaging Shared Resource for assistance with microscopy and image analysis and members of the Henikoff lab for helpful discussions. This work was supported by the Howard Hughes Medical Institute (to S.H.) and NIH Ruth L. Kirschstein National Research Service Award 1F32GM153148-01 (to S.M.L.). *Author contributions:* S.M.L., K.A, and S.H. designed the study. S.M.L. performed the experiments and analyzed the data. K.A. and S.H. supervised the study. S.M.L wrote the original draft and all authors reviewed and approved the manuscript.

References

Aguilera J, Duan J, Cortez K, Lee RS, Aragon A, Ray M, Larschan E. 2025. The CLAMP GA-binding transcription factor regulates heat stress-induced transcriptional repression by associating with 3D chromatin loops. *bioRxiv* doi:10.1101/2023.10.08.561401.

Akkouche A, Kneuss E, Bornelov S, Renaud Y, Eastwood EL, van Lopik J, Gueguen N, Jiang M, Creixell P, Maupetit-Mehouas S et al. 2025. Binding of heterochromatin protein Rhino to a subset of piRNA clusters depends on a combination of two histone marks. *Nat Struct Mol Biol* **32**: 1517-1527.

Altman DG, Bland JM. 1983. Measurement in Medicine: The Analysis of Method Comparison Studies. *The Statistician* **32**: 307-317.

Amemiya HM, Kundaje A, Boyle AP. 2019. The ENCODE Blacklist: Identification of Problematic Regions of the Genome. *Sci Rep* **9**: 9354.

Biteau B, Hochmuth CE, Jasper H. 2008. JNK activity in somatic stem cells causes loss of tissue homeostasis in the aging Drosophila gut. *Cell Stem Cell* **3**: 442-455.

Biteau B, Jasper H. 2014. Slit/Robo signaling regulates cell fate decisions in the intestinal stem cell lineage of Drosophila. *Cell Rep* **7**: 1867-1875.

Blackledge NP, Klose RJ. 2021. The molecular principles of gene regulation by Polycomb repressive complexes. *Nat Rev Mol Cell Biol* **22**: 815-833.

Boyer LA, Plath K, Zeitlinger J, Brambrink T, Medeiros LA, Lee TI, Levine SS, Wernig M, Tajonar A, Ray MK et al. 2006. Polycomb complexes repress developmental regulators in murine embryonic stem cells. *Nature* **441**: 349-353.

Brown JL, Sun MA, Kassis JA. 2018. Global changes of H3K27me3 domains and Polycomb group protein distribution in the absence of recruiters Spps or Pho. *Proc Natl Acad Sci U S A* **115**: E1839-E1848.

Buchon N, Osman D, David FP, Fang HY, Boquete JP, Deplancke B, Lemaitre B. 2013. Morphological and molecular characterization of adult midgut compartmentalization in Drosophila. *Cell Rep* **3**: 1725-1738.

Butler A, Hoffman P, Smibert P, Papalexi E, Satija R. 2018. Integrating single-cell transcriptomic data across different conditions, technologies, and species. *Nat Biotechnol* **36**: 411-420.

Cao R, Wang L, Wang H, Xia L, Erdjument-Bromage H, Tempst P, Jones RS, Zhang Y. 2002. Role of histone H3 lysine 27 methylation in Polycomb-group silencing. *Science* **298**: 1039-1043.

Capo F, Wilson A, Di Cara F. 2019. The Intestine of Drosophila melanogaster: An Emerging Versatile Model System to Study Intestinal Epithelial Homeostasis and Host-Microbial Interactions in Humans. *Microorganisms* **7**.

Clark RI, Salazar A, Yamada R, Fitz-Gibbon S, Morselli M, Alcaraz J, Rana A, Rera M, Pellegrini M, Ja WW et al. 2015. Distinct Shifts in Microbiota Composition during Drosophila Aging Impair Intestinal Function and Drive Mortality. *Cell Rep* **12**: 1656-1667.

Danecek P, Bonfield JK, Liddle J, Marshall J, Ohan V, Pollard MO, Whitwham A, Keane T, McCarthy SA, Davies RM et al. 2021. Twelve years of SAMtools and BCFtools. *Gigascience* **10**: giab008.

Denecke S, Fusetto R, Batterham P. 2017. Describing the role of Drosophila melanogaster ABC transporters in insecticide biology using CRISPR-Cas9 knockouts. *Insect Biochem Mol Biol* **91**: 1-9.

Denell RE, Frederick RD. 1983. Homoeosis in Drosophila: a description of the Polycomb lethal syndrome. *Dev Biol* **97**: 34-47.

Dutta D, Dobson AJ, Houtz PL, Glasser C, Revah J, Korzelius J, Patel PH, Edgar BA, Buchon N. 2015. Regional Cell-Specific Transcriptome Mapping Reveals Regulatory Complexity in the Adult Drosophila Midgut. *Cell Rep* **12**: 346-358.

El Mai M, Bird M, Allouche A, Targen S, Serifoglu N, Lopes-Bastos B, Guigonis JM, Kang D, Pourcher T, Yue JX et al. 2023. Gut-specific telomerase expression counteracts systemic aging in telomerase-deficient zebrafish. *Nat Aging* **3**: 567-584.

Emerson FJ, Lee SS. 2023. Chromatin: the old and young of it. *Front Mol Biosci* **10**: 1270285.

Feser J, Truong D, Das C, Carson JJ, Kieft J, Harkness T, Tyler JK. 2010. Elevated histone expression promotes life span extension. *Mol Cell* **39**: 724-735.

Granja JM, Corces MR, Pierce SE, Bagdatli ST, Choudhry H, Chang HY, Greenleaf WJ. 2021. ArchR is a scalable software package for integrative single-cell chromatin accessibility analysis. *Nat Genet* **53**: 403-411.

Grant CE, Bailey TL, Noble WS. 2011. FIMO: scanning for occurrences of a given motif. *Bioinformatics* **27**: 1017-1018.

Havas A, Yin S, Adams PD. 2022. The role of aging in cancer. *Molecular oncology* **16**: 3213-3219.

Henikoff S, Henikoff JG, Kaya-Okur HS, Ahmad K. 2020. Efficient chromatin accessibility mapping in situ by nucleosome-tethered tagmentation. *Elife* **9**: e63274.

Henikoff S, Zheng Y, Paranal RM, Xu Y, Greene JE, Henikoff JG, Russell ZR, Szulzewsky F, Thirimanne HN, Kugel S et al. 2025. RNA polymerase II at histone genes predicts outcome in human cancer. *Science* **387**: 737-743.

Huang SK, Whitney PH, Dutta S, Shvartsman SY, Rushlow CA. 2021. Spatial organization of transcribing loci during early genome activation in Drosophila. *Curr Biol* **31**: 5102-5110 e5105.

Hung RJ, Hu Y, Kirchner R, Liu Y, Xu C, Comjean A, Tattikota SG, Li F, Song W, Ho Sui S et al. 2020. A cell atlas of the adult Drosophila midgut. *Proc Natl Acad Sci U S A* **117**: 1514-1523.

Janssens DH, Greene JE, Wu SJ, Codomo CA, Minot SS, Furlan SN, Ahmad K, Henikoff S. 2024. Scalable single-cell profiling of chromatin modifications with sciCUT&Tag. *Nat Protoc* **19**: 83-112.

Janssens DH, Otto DJ, Meers MP, Setty M, Ahmad K, Henikoff S. 2022. CUT&Tag2for1: a modified method for simultaneous profiling of the accessible and silenced regulome in single cells. *Genome Biol* **23**: 81.

Jenkins NL, McColl G, Lithgow GJ. 2004. Fitness cost of extended lifespan inCaenorhabditis elegans. *Proceedings of the Royal Society of London Series B: Biological Sciences* **271**: 2523-2526.

Jiang H, Patel PH, Kohlmaier A, Grenley MO, McEwen DG, Edgar BA. 2009. Cytokine/Jak/Stat signaling mediates regeneration and homeostasis in the Drosophila midgut. *Cell* **137**: 1343-1355.

Josserand M, Rubanova N, Stefanutti M, Roumeliotis S, Espenel M, Marshall OJ, Servant N, Gervais L, Bardin AJ. 2023. Chromatin state transitions in the Drosophila intestinal lineage identify principles of cell-type specification. *Dev Cell* **58**: 3048-3063 e3046.

Kassis JA, Kennison JA, Tamkun JW. 2017. Polycomb and Trithorax Group Genes in Drosophila. *Genetics* **206**: 1699-1725.

Katheder NS, Browder KC, Chang D, De Maziere A, Kujala P, van Dijk S, Klumperman J, Lu TC, Li H, Lai Z et al. 2023. Nicotinic acetylcholine receptor signaling maintains epithelial barrier integrity. *Elife* **12**: e86381.

Kaya-Okur HS, Janssens DH, Henikoff JG, Ahmad K, Henikoff S. 2020. Efficient low-cost chromatin profiling with CUT&Tag. *Nat Protoc* **15**: 3264-3283.

Kaya-Okur HS, Wu SJ, Codomo CA, Pledger ES, Bryson TD, Henikoff JG, Ahmad K, Henikoff S. 2019. CUT&Tag for efficient epigenomic profiling of small samples and single cells. *Nat Commun* **10**: 1930.

Kent WJ, Zweig AS, Barber G, Hinrichs AS, Karolchik D. 2010. BigWig and BigBed: enabling browsing of large distributed datasets. *Bioinformatics* **26**: 2204-2207.

Kim YK, Cho B, Cook DP, Trcka D, Wrana JL, Ramalho-Santos M. 2023. Absolute scaling of single-cell transcriptomes identifies pervasive hypertranscription in adult stem and progenitor cells. *Cell Rep* **42**: 111978.

Kim YK, Collignon E, Martin SB, Ramalho-Santos M. 2024. Hypertranscription: the invisible hand in stem cell biology. *Trends Genet* **40**: 1032-1046.

Konno K, Mitsuhashi W. 2019. The peritrophic membrane as a target of proteins that play important roles in plant defense and microbial attack. *J Insect Physiol* **117**: 103912.

Krause SA, Overend G, Dow JAT, Leader DP. 2022. FlyAtlas 2 in 2022: enhancements to the Drosophila melanogaster expression atlas. *Nucleic Acids Res* **50**: D1010-D1015.

Langmead B, Salzberg SL. 2012. Fast gapped-read alignment with Bowtie 2. *Nat Methods* **9**: 357-359.

Leader DP, Krause SA, Pandit A, Davies SA, Dow JAT. 2018. FlyAtlas 2: a new version of the Drosophila melanogaster expression atlas with RNA-Seq, miRNA-Seq and sex-specific data. *Nucleic Acids Res* **46**: D809-D815.

Lehane MJ. 1997. Peritrophic matrix structure and function. *Annu Rev Entomol* **42**: 525-550.

Li H, Qi Y, Jasper H. 2016. Preventing Age-Related Decline of Gut Compartmentalization Limits Microbiota Dysbiosis and Extends Lifespan. *Cell Host Microbe* **19**: 240-253.

Liang J, Balachandra S, Ngo S, O'Brien LE. 2017. Feedback regulation of steady-state epithelial turnover and organ size. *Nature* **548**: 588-591.

Lim JG, Fuller MT. 2012. Somatic cell lineage is required for differentiation and not maintenance of germline stem cells in Drosophila testes. *Proc Natl Acad Sci U S A* **109**: 18477-18481.

Loubiere V, Delest A, Thomas A, Bonev B, Schuettengruber B, Sati S, Martinez AM, Cavalli G. 2016. Coordinate redeployment of PRC1 proteins suppresses tumor formation during Drosophila development. *Nat Genet* **48**: 1436-1442.

Ma Z, Wang H, Cai Y, Wang H, Niu K, Wu X, Ma H, Yang Y, Tong W, Liu F et al. 2018. Epigenetic drift of H3K27me3 in aging links glycolysis to healthy longevity in Drosophila. *Elife* **7**: e35368.

Mahat DB, Tippens ND, Martin-Rufino JD, Waterton SK, Fu J, Blatt SE, Sharp PA. 2024. Single-cell nascent RNA sequencing unveils coordinated global transcription. *Nature* **631**: 216-223.

Martin M. 2011. Cutadapt removes adapter sequences from high-throughput sequencing reads. *EMBnetjournal* **17**: 1138-1143.

Martins RR, McCracken AW, Simons MJP, Henriques CM, Rera M. 2018. How to Catch a Smurf? - Ageing and Beyond... In vivo Assessment of Intestinal Permeability in Multiple Model Organisms. *Bio Protoc* **8**.

Marzluff WF, Koreski KP. 2017. Birth and Death of Histone mRNAs. *Trends Genet* **33**: 745-759.

Meers MP, Tenenbaum D, Henikoff S. 2019. Peak calling by Sparse Enrichment Analysis for CUT&RUN chromatin profiling. *Epigenetics Chromatin* **12**: 42.

Metchnikoff E, Mitchell P. 1907. *The prolongation of life; optimistic studies*. G.P. Putnam Sons, London.

Micchelli CA, Perrimon N. 2006. Evidence that stem cells reside in the adult Drosophila midgut epithelium. *Nature* **439**: 475-479.

Niccoli T, Partridge L. 2012. Ageing as a risk factor for disease. *Curr Biol* **22**: R741-752.

Ohlstein B, Spradling A. 2006. The adult Drosophila posterior midgut is maintained by pluripotent stem cells. *Nature* **439**: 470-474.

Orsi GA, Kasinathan S, Hughes KT, Saminadin-Peter S, Henikoff S, Ahmad K. 2014. High-resolution mapping defines the cooperative architecture of Polycomb response elements. *Genome Res* **24**: 809-820.

Parreno V, Loubiere V, Schuettengruber B, Fritsch L, Rawal CC, Erokhin M, Gyorffy B, Normanno D, Di Stefano M, Moreaux J et al. 2024. Transient loss of Polycomb components induces an epigenetic cancer fate. *Nature* **629**: 688-696.

Quinlan AR. 2014. BEDTools: The Swiss-Army Tool for Genome Feature Analysis. *Curr Protoc Bioinformatics* **47**: 11 12 11-34.

R Core Team. 2025. R: A Language and Environment for Statistical Computing. R Foundation for Statistical Computing, Vienna, Austria.

Ramirez F, Ryan DP, Gruning B, Bhardwaj V, Kilpert F, Richter AS, Heyne S, Dundar F, Manke T. 2016. deepTools2: a next generation web server for deep-sequencing data analysis. *Nucleic Acids Res* **44**: W160-165.

Rauluseviciute I, Riudavets-Puig R, Blanc-Mathieu R, Castro-Mondragon JA, Ferenc K, Kumar V, Lemma RB, Lucas J, Cheneby J, Baranasic D et al. 2024. JASPAR 2024: 20th anniversary of the open-access database of transcription factor binding profiles. *Nucleic Acids Res* **52**: D174-D182.

Rera M, Bahadorani S, Cho J, Koehler CL, Ulgherait M, Hur JH, Ansari WS, Lo T, Jr., Jones DL, Walker DW. 2011. Modulation of longevity and tissue homeostasis by the Drosophila PGC-1 homolog. *Cell Metab* **14**: 623-634.

Rera M, Clark RI, Walker DW. 2012. Intestinal barrier dysfunction links metabolic and inflammatory markers of aging to death in Drosophila. *Proc Natl Acad Sci U S A* **109**: 21528-21533.

Rodriguez-Fernandez IA, Tauc HM, Jasper H. 2020. Hallmarks of aging Drosophila intestinal stem cells. *Mech Ageing Dev* **190**: 111285.

Salazar AM, Aparicio R, Clark RI, Rera M, Walker DW. 2023. Intestinal barrier dysfunction: an evolutionarily conserved hallmark of aging. *Dis Model Mech* **16**: dmm049969.

Schaaf CA, Misulovin Z, Gause M, Koenig A, Gohara DW, Watson A, Dorsett D. 2013. Cohesin and polycomb proteins functionally interact to control transcription at silenced and active genes. *PLoS Genet* **9**: e1003560.

Schindelin J, Arganda-Carreras I, Frise E, Kaynig V, Longair M, Pietzsch T, Preibisch S, Rueden C, Saalfeld S, Schmid B et al. 2012. Fiji: an open-source platform for biological-image analysis. *Nat Methods* **9**: 676-682.

Schwartz YB, Kahn TG, Nix DA, Li XY, Bourgon R, Biggin M, Pirrotta V. 2006. Genome-wide analysis of Polycomb targets in Drosophila melanogaster. *Nat Genet* **38**: 700-705.

Siebold AP, Banerjee R, Tie F, Kiss DL, Moskowitz J, Harte PJ. 2010. Polycomb Repressive Complex 2 and Trithorax modulate Drosophila longevity and stress resistance. *Proc Natl Acad Sci U S A* **107**: 169-174.

Siudeja K, van den Beek M, Riddiford N, Boumard B, Wurmser A, Stefanutti M, Lameiras S, Bardin AJ. 2021. Unraveling the features of somatic transposition in the Drosophila intestine. *EMBO J* **40**: e106388.

Sun D, Luo M, Jeong M, Rodriguez B, Xia Z, Hannah R, Wang H, Le T, Faull KF, Chen R et al. 2014. Epigenomic profiling of young and aged HSCs reveals concerted changes during aging that reinforce self-renewal. *Cell Stem Cell* **14**: 673-688.

Tauc HM, Rodriguez-Fernandez IA, Hackney JA, Pawlak M, Ronnen Oron T, Korzelius J, Moussa HF, Chaudhuri S, Modrusan Z, Edgar BA et al. 2021. Age-related changes in polycomb gene regulation disrupt lineage fidelity in intestinal stem cells. *Elife* **10**: e62250.

Wickham H. 2016. ggplot2 : Elegant Graphics for Data Analysis. In *Use R!,*, doi:10.1007/978-3-319-24277-4, pp. 1 online resource (XVI, 260 pages 232 illustrations, 140 illustrations in color. Springer International Publishing : Imprint: Springer,, Cham.

Williams GC. 1957. Pleiotropy, Natural Selection, and the Evolution of Senescence. *Evolution* **11**: 398-411.

Wu SJ, Furlan SN, Mihalas AB, Kaya-Okur HS, Feroze AH, Emerson SN, Zheng Y, Carson K, Cimino PJ, Keene CD et al. 2021. Single-cell CUT&Tag analysis of chromatin modifications in differentiation and tumor progression. *Nat Biotechnol* **39**: 819-824.

Yang N, Occean JR, Melters DP, Shi C, Wang L, Stransky S, Doyle ME, Cui CY, Delannoy M, Fan J et al. 2023. A hyper-quiescent chromatin state formed during aging is reversed by regeneration. *Mol Cell* **83**: 1659-1676 e1611.

Yu G, Wang LG, Han Y, He QY. 2012. clusterProfiler: an R package for comparing biological themes among gene clusters. *OMICS* **16**: 284-287.

Zabidi MA, Arnold CD, Schernhuber K, Pagani M, Rath M, Frank O, Stark A. 2015. Enhancer-core-promoter specificity separates developmental and housekeeping gene regulation. *Nature* **518**: 556-559.

Zhang C, Ding Y, Zhou M, Tang Y, Chen R, Chen Y, Wen Y, Wang S. 2023. RNAi-mediated CHS-2 silencing affects the synthesis of chitin and the formation of the peritrophic membrane in the midgut of Aedes albopictus larvae. *Parasit Vectors* **16**: 259.

Zheng Y, Ahmad K, Henikoff S. 2025. Total whole-arm chromosome losses predict malignancy in human cancer. *Proc Natl Acad Sci U S A* **122**: e2505385122.

Zhu H, Ludington WB, Spradling AC. 2024. Cellular and molecular organization of the Drosophila foregut. *Proc Natl Acad Sci U S A* **121**: e2318760121.

Zhuang X, Wang Q, Joost S, Ferrena A, Humphreys DT, Li Z, Blum M, Krause K, Ding S, Landais Y et al. 2025. Ageing limits stemness and tumorigenesis by reprogramming iron homeostasis. *Nature* **637**: 184-194.

Figure Legends

Figure 1. Repressed landscapes for cell types in the Drosophila gut.

876 *(A)* Immunofluorescence image of the gut in a young *esgGal4/CyO; UAS-GFP/TM6B*
877 female**.** GFP (green) marks stem cells and enteroblasts, red anti-H3K27me3, DAPI in
878 grey. Pink arrowhead points to ISC/EBs, blue arrowhead points to enterocytes, and yellow
879 arrowhead points to enteroendocrine cells. Enterocytes are the large DAPI stained nuclei
880 (blue arrow). Enteroendocrine cells are identified by their small nucleus size in relation to
881 the larger enterocytes and low GFP signal (yellow arrows). (*B*) UMAP of H3K27me3
882 signal in gut cells from 1-, 15-, and 40-day-old females. Clusters are assigned cell types
883 by low CSS score at marker genes. (*C*) Violin plots of the distribution of fragments per
884 cell for 1-day-old cell types. (*D*) Log_2 transformed counts per kilobase per million (CPKM)
885 normalized and *Z*-score normalized heatmaps from differential analysis of H3K27me3
886 over genes between 1day old cell types. (*E-H*) UCSC Genome Browser tracks of
887 repressed domains in the three cell types in young guts. (*E*) The *ANTP-C* domain is
888 shared between all three cell types. (*F*) A domain encompassing the piRNA cluster *42AB*
889 is present only in ISC/EBs, (*G*) a domain encompassing the *lncRNA:CR32773* gene is
890 present only in enteroendocrine cells, and (*H*) a domain encompassing the *how* gene is
891 present only in enterocytes.

892

893 **Figure 2. Changes in repressed landscapes in gut cells with age.**

894 (*A-C*) UMAPs of cell types from guts of different ages. Enteroendocrine cells and
895 ISC/EBs of different ages are mixed within cell type clusters, but enterocytes form three
896 separate clusters. (*D-F*) *Z*-score normalized heatmaps from differential analysis of
897 H3K27me3 signal over genes between young and old cells. The first column of each
898 heatmap is the log_2 transformed counts per kilobase per million (CPKM) for 1-day old

cells for each cell type. (*D*) ISC/EBs have an almost equal number of genes that lose (39 genes) and gain (36 genes) H3K27me3 signal with age. (*E*) Enteroendocrine cells show a greater number of losses of H3K27me3 signal (237 genes) compared to a gain in H3K27me3 signal (40 genes) with age. (*E*) Enterocytes have the greatest number of genes that show a change in H3K27me3 signal with age (1588 genes) with an age-related gain in H3K27me3 signal in 878 genes. It should be noted that genes that gain H3K27me3 signal are weak domains in young cells and genes that show a loss of H3K27me3 signal are strong domains in young cells. (*G,H*) Genome browser tracks of genes that are differentially methylated in enterocytes, showing a loss (*G*) and gain (*H*) in H3K27me3 signal with age.

Figure 3. Repression of barrier genes in aged enterocytes.

(*A*) Results of a Smurf assay in which flies are fed food containing a non-absorbable blue dye. Fly on the left is 1 day old and has the blue dye is restricted to the digestive tract. Fly on the right is 40 days old and the blue dye can be seen throughout the entire body. (*B*) Top four GO terms on genes that gain H3K27me3 signal in aged enterocytes from differential analysis. (*C-D*) UCSC Genome Browser tracks of chitin synthesis (*C*) and chitinase (*D*) genes that form new H3K27me3 domains in aged enterocytes. (*E*) Row *z*-score normalized heatmap of RNAPIIS5P counts over chitin synthesis gene promoters. The first column of each heatmap is the $\log_2$ transformed counts for 1-day old tissue for each promoter. Row *z*-scoring is used to present directionality of the change in signal with age. (*F-G*) UCSC Genome Browser track of Polycomb in 1-dayold guts at the

promoter of the *Chs2* gene (*F*) and at *Cht9* (*G*). (*H*) Heatmap of $\log_2$ transformed counts for Polycomb binding at each chitin synthesis gene promoter.

Figure 4. Stem cells display overproliferation and derepression of lineage-specifying genes and JAK/STAT ligands.

(*A*) Row *z*-score normalized heatmap of H3K27me3 counts of ISC/EBs for enteroendocrine genes defined in Fig. 1D. The first column is the $\log_2$ transformed counts per kilobase per million (CPKM) for 1-day old tissue for each gene. (*B*) Immunofluorescence image of the gut in a young (1 day old) and old (40 days old) *esgGal4/CyO; UAS-GFP/TM6B* female**.** GFP (green) marks stem cells and enteroblasts and DAPI in grey. (*C*) Pie charts of the proportion of each cell type per age. Significance was assessed by Monte Carlo permutation test (10,000 permutations). Observed enrichment was greater than expected by chance ($p < 0.0001$).(*D*) Row *z*-score normalized heatmap of H3K27me3 counts over the *Unpaired* domain, which encompasses three genes encoding JAK/STAT ligands**.** The first column is the $\log_2$ transformed counts for 1-day old tissue for each promoter. ISC/EBs have the lowest H3K27me3 level of the three cell types in 1-day old tissue and lose H3K27me3 signal with age, indicating derepression. Row *z*-scoring is used to present directionality of the change in signal with age. (*E*) Row *z*-score normalized heatmap of RNAPIIS5P counts over promoters of the *Upd1*, *Upd2*, and *Upd3* genes. The first column is the $\log_2$ transformed counts for 1-day old tissue for each promoter. *Upd2* and *Upd3* gain RNAPIIS5P signal in aged tissues which is consistent with previous reports of these ligands. Row *z*-scoring is used to present directionality of the change in signal with age.

Figure 5. S-phase histone genes are upregulated with global downregulation in aged guts.

(*A*) RNAPIIS5P counts for the absolute difference (40 days old– 15 days old) counts versus average count ($\log_{10}$(40 days old + 15 days old)/2) for all promoters in the Drosophila genome. (*B*) UCSC Genome Browser track of RNAPIIS5P at a representative histone gene repeat. Yellow boxes highlight the promoter region of each histone gene. (*C*) Bar charts depicting RNAPIIS5P counts per million (CPM) for each promoter of the histone gene repeat shown in panel (*B*). Significance was assessed Poisson rate test compared to 15 days old samples with asterisks indicating $p < 0.05$ (*), $p < 0.01$ (**), $p < 0.001$ (***), and $p < 0.0001$ (****).

Figure 6. Model for cell-type-specific Polycomb remodeling drives gut aging.

(*A*) Young gut: The epithelium is composed primarily of enterocytes, with a small population of ISC/EBs. In enterocytes, Polycomb (Pc) binds chitin-related promoters (e.g., *Chs2*, *Cht* cluster) but H3K27me3 levels remain low, allowing robust RNAPII occupancy and continuous peritrophic-matrix production. Stem cells proliferate at homeostatic rates and show low RNAPII occupancy at S-phase histone loci.

(B) Mid-age gut: Enterocyte numbers decline while ISC/EBs expand. H3K27me3 signal accumulates at Pc-bound chitin genes in enterocytes, partially repressing chitin synthesis. The peritrophic matrix becomes thinned, causing moderate luminal stress and a slight increase in enterocyte turnover. Stem cells respond with increased proliferation but maintain low RNAPII at S-phase histone genes.

(C) Old gut: Enterocytes are markedly depleted and ISC/EBs predominate. In enterocytes, broad Pc-nucleated H3K27me3 domains entirely silence chitin-related loci,

967 weakening the peritrophic matrix and exposing the epithelium to high luminal stress,
968 further reducing enterocyte numbers. Barrier failure triggers stem cell hyperproliferation
969 and massive RNAPII accumulation at S-phase histone loci—a histone hypertranscription
970 signature resembling that of aggressive tumors.
971

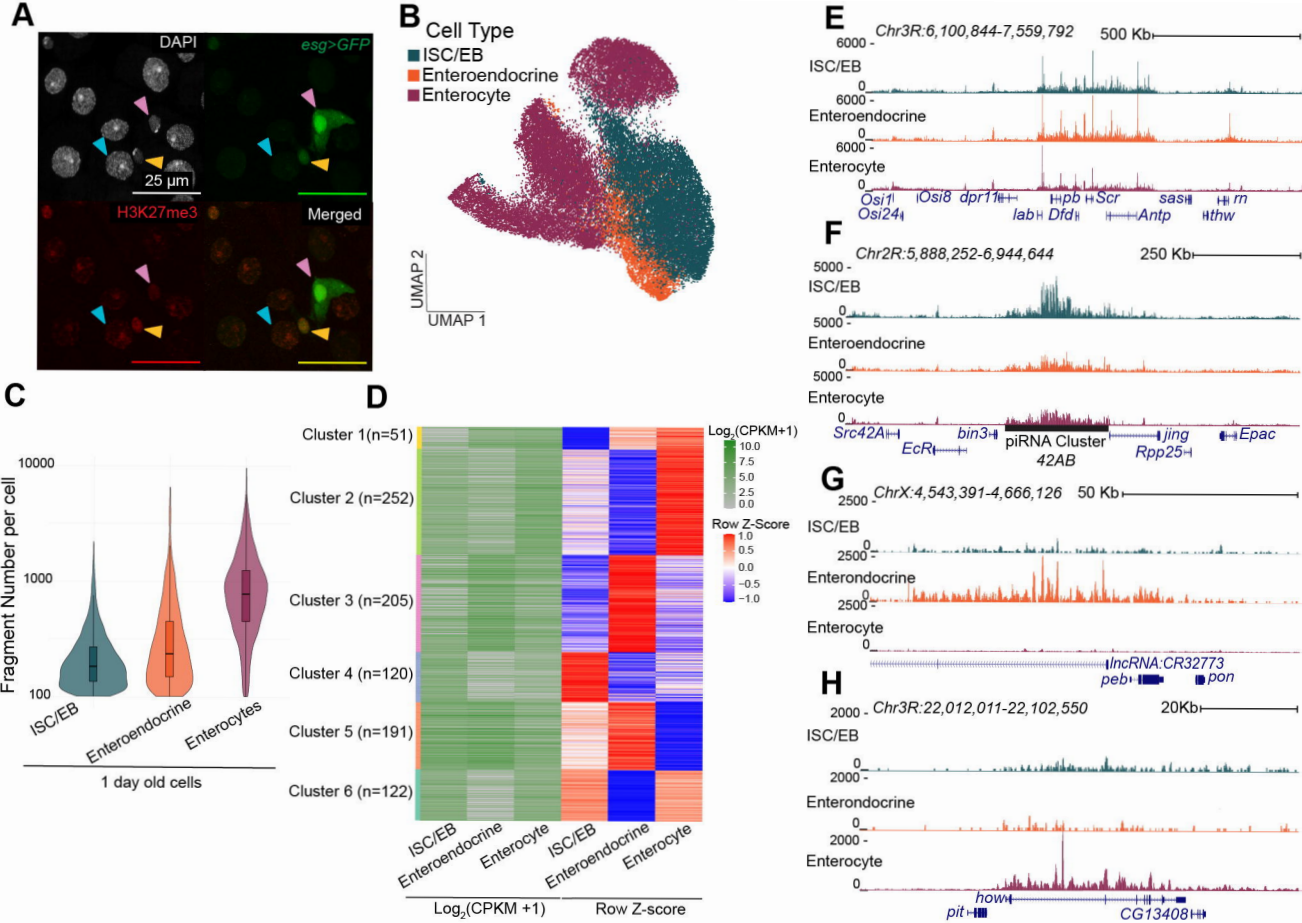
A
DAPI
esg>GFP
25 µm
H3K27me3
Merged
B
Cell Type
ISC/EB
Enteroendocrine
Enterocyte
UMAP 2
UMAP 1
C
Fragment Number per cell
10000
1000
100
ISC/EB
Enteroendocrine
Enterocytes
1 day old cells
D
Cluster 1(n=51)
Cluster 2 (n=252)
Cluster 3 (n=205)
Cluster 4 (n=120)
Cluster 5 (n=191)
Cluster 6 (n=122)
Log2(CPKM+1)
10.0
7.5
5.0
2.5
0.0
Row Z-Score
1.0
0.5
0.0
−0.5
−1.0
ISC/EB
Enteroendocrine
Enterocyte
ISC/EB
Enteroendocrine
Enterocyte
Log2(CPKM +1)
Row Z-score
E
Chr3R:6,100,844-7,559,792
500 Kb
6000
ISC/EB
0
6000
Enteroendocrine
0
6000
Enterocyte
0
Osi1
Osi8
dpr11
hpb
Scr
sasi
rn
Osi24
lab
Dfd
Antp
thw
F
Chr2R:5,888,252-6,944,644
250 Kb
5000
ISC/EB
0
5000
Enteroendocrine
0
5000
Enterocyte
0
Src42A
bin3
piRNA Cluster
42AB
jing
Epac
EcR
Rpp25
G
ChrX:4,543,391-4,666,126
50 Kb
2500
ISC/EB
0
2500
Enterondocrine
0
2500
Enterocyte
0
lncRNA:CR32773
peb
pon
H
2000
Chr3R:22,012,011-22,102,550
20Kb
ISC/EB
0
2000
Enterondocrine
0
2000
Enterocyte
0
how
pit
CG13408

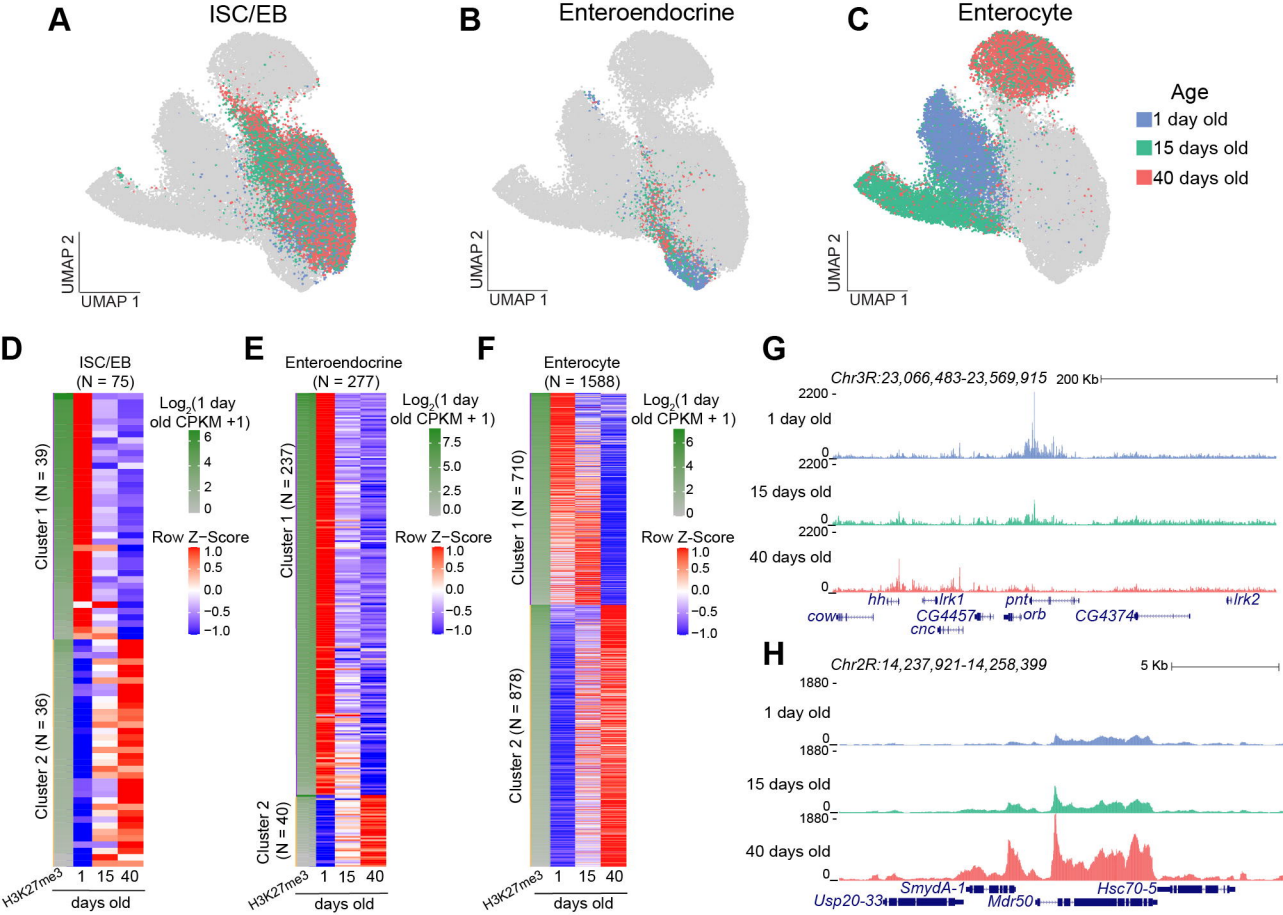
A
ISC/EB
B
Enteroendocrine
C
Enterocyte
Age
1 day old
15 days old
40 days old
UMAP 2
UMAP 1
D
ISC/EB
(N = 75)
Log2(1 day old CPKM +1)
Row Z−Score
Cluster 1 (N = 39)
Cluster 2 (N = 36)
H3K27me3
1 15 40
days old
E
Enteroendocrine
(N = 277)
Log2(1 day old CPKM + 1)
Cluster 1 (N = 237)
Cluster 2 (N = 40)
F
Enterocyte
(N = 1588)
Cluster 1 (N = 710)
Cluster 2 (N = 878)
G
Chr3R:23,066,483-23,569,915
200 Kb
hh
lrk1
pnt
lrk2
cow
CG4457
orb
CG4374
cnc
H
Chr2R:14,237,921-14,258,399
5 Kb
SmydA-1
Hsc70-5
Usp20-33
Mdr50

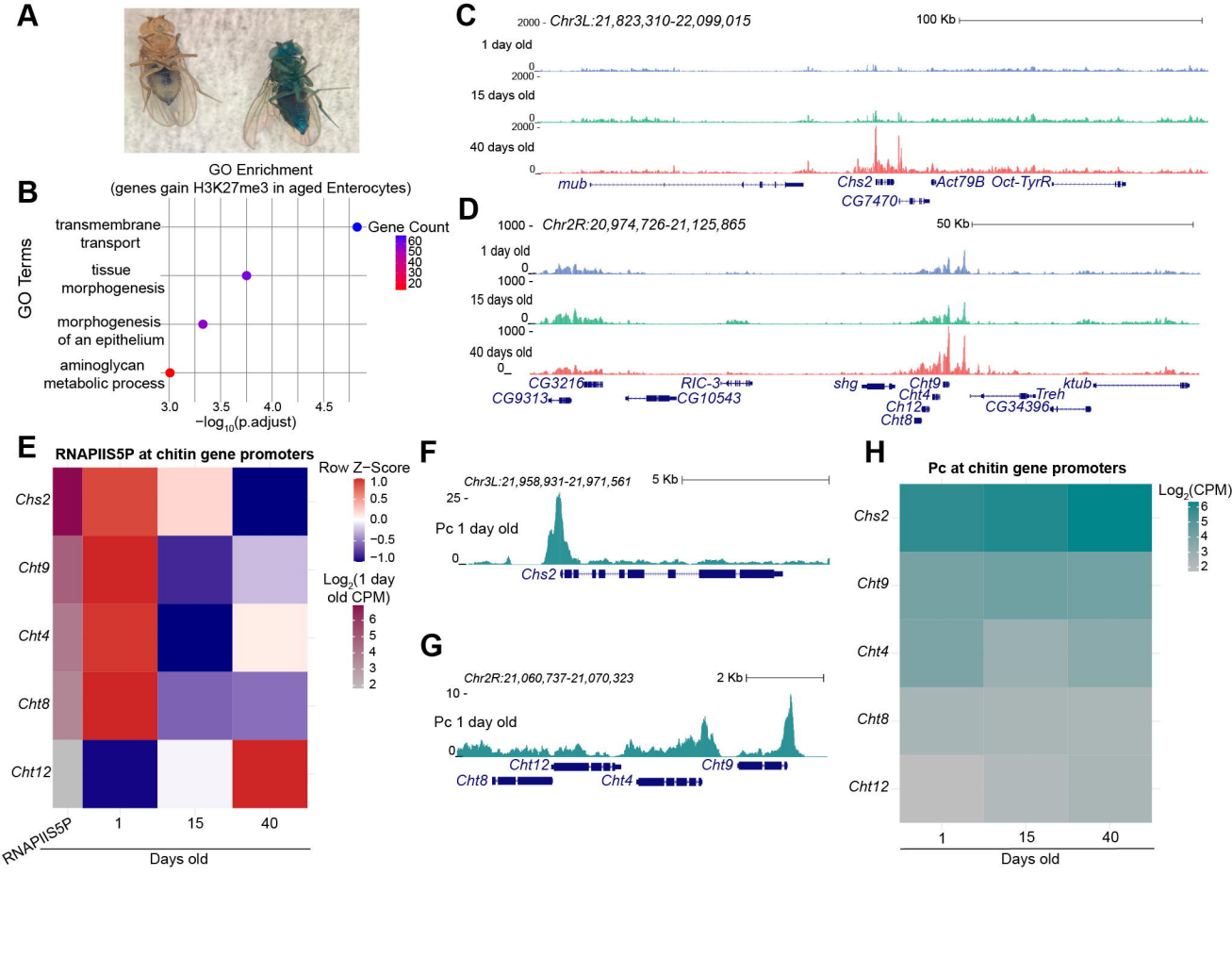
A
B
GO Enrichment
(genes gain H3K27me3 in aged Enterocytes)
GO Terms
transmembrane transport
tissue morphogenesis
morphogenesis of an epithelium
aminoglycan metabolic process
Gene Count
60
50
40
30
20
3.0
3.5
4.0
4.5
−log10(p.adjust)
C
2000 - Chr3L:21,823,310-22,099,015
100 Kb
1 day old
15 days old
40 days old
mub
Chs2
Act79B
Oct-TyrR
CG7470
D
1000 - Chr2R:20,974,726-21,125,865
50 Kb
1 day old
15 days old
40 days old
CG32166
CG9313
RIC-3
CG10543
shg
Cht9
Cht4
Cht12
Cht8
Treh
ktub
CG34396
E
RNAPIIS5P at chitin gene promoters
Row Z−Score
1.0
0.5
0.0
−0.5
−1.0
Log2(1 day old CPM)
6
5
4
3
2
Chs2
Cht9
Cht4
Cht8
Cht12
RNAPIIS5P
1
15
40
Days old
F
Chr3L:21,958,931-21,971,561
5 Kb
25 -
Pc 1 day old
Chs2
G
Chr2R:21,060,737-21,070,323
2 Kb
10 -
Pc 1 day old
Cht12
Cht9
Cht8
Cht4
H
Pc at chitin gene promoters
Log2(CPM)
6
5
4
3
2
Chs2
Cht9
Cht4
Cht8
Cht12
1
15
40
Days old

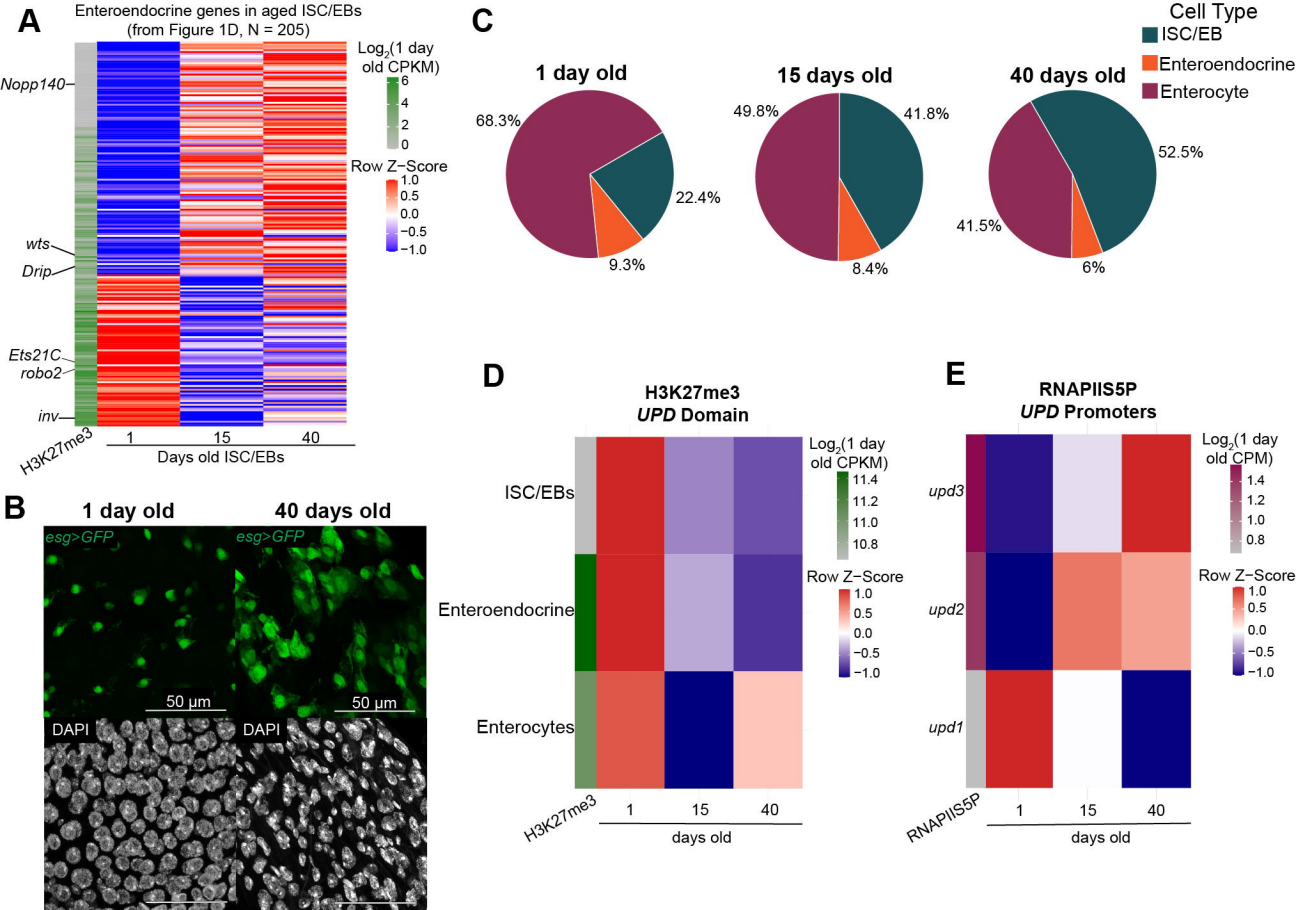
A
Enteroendocrine genes in aged ISC/EBs
(from Figure 1D, N = 205)
Log2(1 day old CPKM)
6
4
2
0
Row Z−Score
1.0
0.5
0.0
−0.5
−1.0
Nopp140
wts
Drip
Ets21C
robo2
inv
H3K27me3
1
15
40
Days old ISC/EBs
B
1 day old
40 days old
esg>GFP
esg>GFP
50 µm
50 µm
DAPI
DAPI
C
Cell Type
ISC/EB
Enteroendocrine
Enterocyte
1 day old
68.3%
22.4%
9.3%
15 days old
49.8%
41.8%
8.4%
40 days old
52.5%
41.5%
6%
D
H3K27me3
UPD Domain
ISC/EBs
Enteroendocrine
Enterocytes
Log2(1 day old CPKM)
11.4
11.2
11.0
10.8
Row Z−Score
1.0
0.5
0.0
−0.5
−1.0
H3K27me3
1
15
40
days old
E
RNAPIIS5P
UPD Promoters
upd3
upd2
upd1
Log2(1 day old CPM)
1.4
1.2
1.0
0.8
Row Z−Score
1.0
0.5
0.0
−0.5
−1.0
RNAPIIS5P
1
15
40
days old

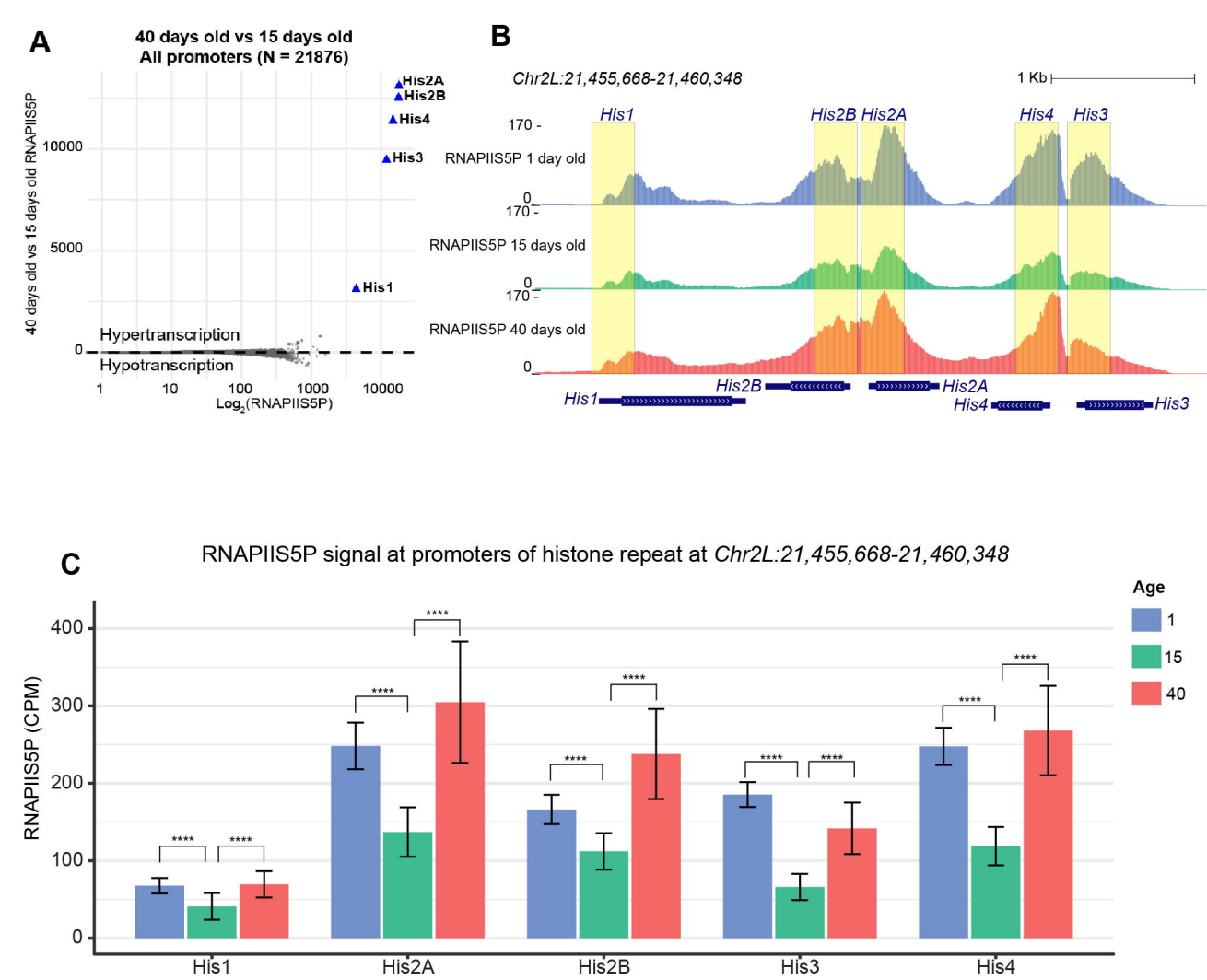
A
40 days old vs 15 days old
All promoters (N = 21876)
His2A
His2B
His4
His3
His1
Hypertranscription
Hypotranscription
40 days old vs 15 days old RNAPIIS5P
Log2(RNAPIIS5P)
B
Chr2L:21,455,668-21,460,348
1 Kb
His1
His2B
His2A
His4
His3
RNAPIIS5P 1 day old
RNAPIIS5P 15 days old
RNAPIIS5P 40 days old
C
RNAPIIS5P signal at promoters of histone repeat at Chr2L:21,455,668-21,460,348
RNAPIIS5P (CPM)
Age
1
15
40
His1
His2A
His2B
His3
His4

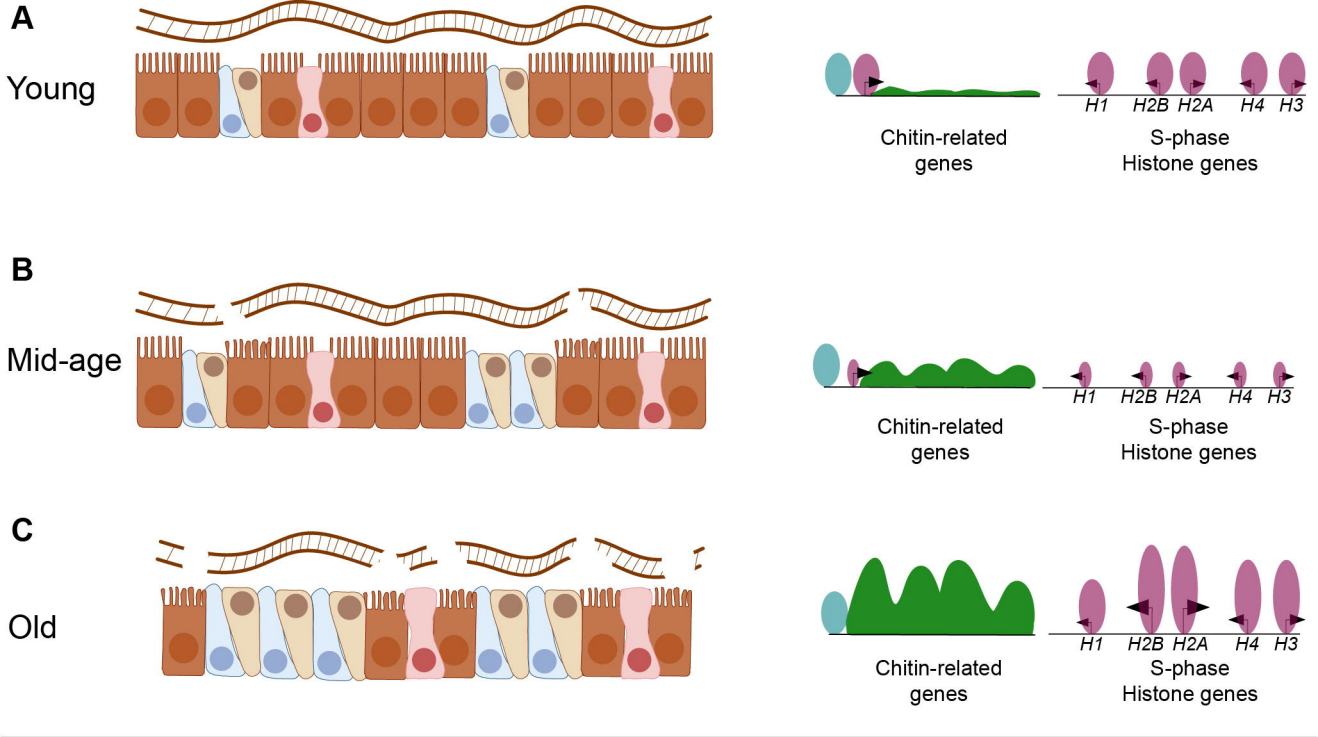
A
Young
Chitin-related genes
H1 H2B H2A H4 H3
S-phase Histone genes
B
Mid-age
Chitin-related genes
H1 H2B H2A H4 H3
S-phase Histone genes
C
Old
Chitin-related genes
H1 H2B H2A H4 H3
S-phase Histone genes
Enterocyte
Intestinal Stem Cell
Enteroblast
Enteroendocrine cell
Chitinous Peritrophic Matrix
Weakened Chitinous Peritrophic Matrix
Pc protein
RNAPIIS5P
H3K27me3

Polycomb misregulation in enterocytes drives tissue decline in the aging *Drosophila* intestine

Sarah Leichter, Kami Ahmad and Steve Henikoff

Genome Res. published online November 17, 2025
Access the most recent version at doi:10.1101/gr.281058.125